AIP | Physics of Fluids

An immersed boundary method for two-phase fluids and gels and the swimming of Caenorhabditis elegans through viscoelastic fluids

Pilhwa Lee and Charles W. Wolgemuth

Citation: Physics of Fluids **28**, 011901 (2016); doi: 10.1063/1.4938174
View online: http://dx.doi.org/10.1063/1.4938174
View Table of Contents: http://scitation.aip.org/content/aip/journal/pof2/28/1?ver=pdfcov
Published by the AIP Publishing

Articles you may be interested in

The two-dimensional flow of a foam through a constriction: Insights from the bubble model
J. Rheol. **58**, 799 (2014); 10.1122/1.4872058

On self-similarity in the drop-filament corner region formed during pinch-off of viscoelastic fluid threads
Phys. Fluids **24**, 083101 (2012); 10.1063/1.4745179

Confined drop motion in viscoelastic two-phase systems
Phys. Fluids **21**, 013102 (2009); 10.1063/1.3054156

Transient drop deformation upon startup of shear in viscoelastic fluids
Phys. Fluids **17**, 123101 (2005); 10.1063/1.2139630

Control of flow through porous media using polymer gels
J. Appl. Phys. **92**, 1143 (2002); 10.1063/1.1487454

This article is copyrighted as indicated in the article. Reuse of AIP content is subject to the terms at: http://scitation.aip.org/termsconditions. Downloaded to IP: 128.196.189.33 On: Wed, 06 Jan 2016 19:05:57

PHYSICS OF FLUIDS **28**, 011901 (2016)

An immersed boundary method for two-phase fluids and gels and the swimming of *Caenorhabditis elegans* through viscoelastic fluids

Pilhwa Lee[1,a)] and Charles W. Wolgemuth[2,b)]
[1]*Department of Molecular and Integrative Physiology, University of Michigan, 2800 Plymouth Rd., Ann Arbor, Michigan 48109, USA*
[2]*Department of Cell Biology and Center for Cell Analysis and Modeling, University of Connecticut Health Center, 263 Farmington Avenue, Farmington, Connecticut 06030-6406, USA and Department of Physics and Molecular and Cellular Biology, University of Arizona, Tucson, Arizona 85721, USA*

(Received 22 May 2015; accepted 4 December 2015; published online 6 January 2016)

The swimming of microorganisms typically involves the undulation or rotation of thin, filamentary objects in a fluid or other medium. Swimming in Newtonian fluids has been examined extensively, and only recently have investigations into microorganism swimming through non-Newtonian fluids and gels been explored. The equations that govern these more complex media are often nonlinear and require computational algorithms to study moderate to large amplitude motions of the swimmer. Here, we develop an immersed boundary method for handling fluid-structure interactions in a general two-phase medium, where one phase is a Newtonian fluid and the other phase is viscoelastic (e.g., a polymer melt or network). We use this algorithm to investigate the swimming of an undulating, filamentary swimmer in 2D (i.e., a sheet). A novel aspect of our method is that it allows one to specify how forces produced by the swimmer are distributed between the two phases of the fluid. The algorithm is validated by comparing theoretical predictions for small amplitude swimming in gels and viscoelastic fluids. We show how the swimming velocity depends on material parameters of the fluid and the interaction between the fluid and swimmer. In addition, we simulate the swimming of *Caenorhabditis elegans* in viscoelastic fluids and find good agreement between the swimming speeds and fluid flows in our simulations and previous experimental measurements. These results suggest that our methodology provides an accurate means for exploring the physics of swimming through non-Newtonian fluids and gels. © *2016 AIP Publishing LLC.* [http://dx.doi.org/10.1063/1.4938174]

I. INTRODUCTION

Microorganisms live in a wide range of habitats, from oceans and lakes to soil, biofilms, and the tissues of our bodies. While the first two of these environments are well described as Newtonian fluids, the latter are much more complex. Biofilms and eukaryotic tissues are often composite media composed of fluid and polymer intermixed. The polymer in these environments can either be connected into a network, as in a gel, or freely diffusing, as in a polymer melt. While some microorganisms cannot penetrate into dense complex environments, others can. Some can even inhabit both and are able to seamlessly move between a Newtonian fluid and a dense polymer gel. Two prime examples are mammalian sperm and *Borrelia burgdorferi*, the bacterium that causes Lyme disease. Mammalian sperm penetrates into and traverses the cervical mucus of the female reproductive tract.[1] Likewise, *B. burgdorferi* can transition from liquid environments into dense polymer or

a)pilee@umich.edu
b)wolg@email.arizona.edu

 ©2016 AIP Publishing LLC

This article is copyrighted as indicated in the article. Reuse of AIP content is subject to the terms at: http://scitation.aip.org/termsconditions. Downloaded to IP: 128.196.189.33 On: Wed, 06 Jan 2016 19:05:57

cell-filled environments like the skin, methylcellulose solutions, and gelatin.[2,3] Another commonly studied swimming microorganism is the nematode *Caenorhabditis elegans*, which moves through a diverse range of environments, including viscoelastic fluids and gels.[4]

How do the rheological properties of the environment affect the swimming of microorganisms? This question has recently received a substantial amount of attention from theoretical and experimental inquiries on swimming through viscoelastic fluids and gels, as well as in shear-thinning fluids. Swimming in non-Newtonian fluids is quite different from that in Newtonian fluids. In Newtonian fluids at low Reynolds number, Taylor showed that the speed of a small amplitude, undulating swimmer is quadratic in the amplitude and linear in the undulation frequency.[5] Lauga extended this formula to cases where the fluid is viscoelastic and showed that viscoelasticity slows a swimmer.[6] Immersed boundary (IB) calculations using a Oldroyd B fluid model, though, predicted that swimmers with an amplitude that increase from head to tail swim faster than they would in a Newtonian fluid.[7] Recent experiments on the swimming of the nematode *C. elegans* show that viscoelasticity in the surrounding environment does slow the swimming of the nematode[8]; however, experiments using rotating helices observed that swimming speed was enhanced by viscoelasticity.[9] More recently, artificial swimmers with either semi-flexible or rigid tails found that speed enhancement or reduction in complex fluids was due to kinematic alterations in the tail dynamics.[10] Based on these seemingly contradictory findings, it remains unclear that what factors control the speed of a swimmer in a non-Newtonian fluid.

In order to begin to understand the motility of microorganisms through complex media, it may be necessary to develop models that can handle a range of different types of non-Newtonian environments and treat them on equal footing. In this paper, we propose a general two-phase model consisting of a Kelvin-Voigt-type material (i.e., the polymer) intermixed with a viscous fluid. Depending on the parameters that are used, this model can describe a range of non-Newtonian media, from viscoelastic fluids to viscoelastic solids and gels. This kind of two-phase model has been used to describe phase separation, biofilms, and intracellular cell mechanics[11–14] among others. The interaction between the undulating swimmer and the external environment is simulated here using an immersed boundary method. This algorithm then provides a means for simulating the motion of thin swimmers in viscoelastic fluids, such as the previously mentioned nematodes, rotating helices, and artificial swimmer,[8–10] in order to identify the physics behind why viscoelasticity differentially alters swimming speed. The same algorithm can also be used to study the motion of bacteria through gel-like environments, such as the mammalian dermis, which is crucial in the pathogenesis of Lyme disease.[3]

Recently, Du *et al.*[15] also developed an immersed boundary method to explore swimming in a two-fluid model, where both fluids were viscous fluids. This algorithm used two connected immersed boundaries to handle the boundary conditions between the swimmer and each fluid. The major novel feature of the immersed boundary method proposed here is that it can handle a much wider range of constitutive relations for the two phases of the fluid while using just a single immersed boundary that can handle a range of assumptions for how the force from the swimmer is allocated between the different phases in the environment.

We show that our algorithm has the same convergence as standard IB methods (i.e., it is between the first and the second order accurate). We then show that our method is able to recapitulate analytical results that have been done recently for small amplitude swimmers in non-Newtonian environments. As a final test of our algorithm, we look at the swimming of *C. elegans* in viscoelastic fluids and compare our results to recent experimental measurements. Of note, we are able to show that our simulations capture the dependence of swimming speed on the rheological properties of the environment while also describing the development of hyperbolic points in the flow profiles near the swimming organism, as has been observed.[8] We then investigate the physical parameters that cause these stagnation points to emerge.

An outline for the paper is as follows: Section II describes the two-phase fluid model for the motion and stresses in the environment. Section III then provides the mathematical description of a sheet immersed in this medium. In Section IV, we describe the numerical implementation of our immersed boundary representation. In Section V, we explore how various physical parameters affect the swimming speed and compare our results to previous work. In Section VI, we simulate the

This article is copyrighted as indicated in the article. Reuse of AIP content is subject to the terms at: http://scitation.aip.org/termsconditions. Downloaded to IP: 128.196.189.33 On: Wed, 06 Jan 2016 19:05:57

swimming of *C. elegans* in viscoelastic fluids. In the Conclusion, we comment on the relevance of our results to the study of microorganism motility.

II. TWO-PHASE VISCOELASTIC MODEL

We consider a two-phase viscoelastic medium on the two-dimensional Eulerian domain Ω_E, similar to what has been used in a number of other contexts.[13,14,16,17] One phase represents polymer and the other phase is a viscous fluid. The dynamics of the polymer volume fraction ϕ is governed by the continuity equation,

$$\frac{\partial \phi}{\partial t} + \nabla \cdot (\phi \boldsymbol{v}_p) = 0 \,, \tag{1}$$

where $\boldsymbol{v}_p$ is the velocity of the polymer. The Reynolds number for microorganism swimming is almost always less than one and typically less than 10^{-2}.[18] For example, many swimming bacteria are a few μm long and swim at speeds on order of 10 μm/s in fluids with viscosities comparable to water. For these cases, the Reynolds number is about 10^{-5}–10^{-4}. For *C. elegans*, which we will discuss later, the cell body is about 1 mm long and they swim at about 0.5 mm/s,[8] giving a Reynolds number of about 0.5. For Reynolds numbers less than one, the inertial terms typically produce only small to negligible effects.[19] We, therefore, ignore inertial terms in the dynamic equations. The velocity of the fluid phase $\boldsymbol{v}_f$ is then determined by the balance between viscous shear forces, hydrostatic pressure forces, and the body force produced by drag between the fluid and polymer. Likewise, the polymer motion is defined by the balance of elastic restoring forces, viscous forces, hydrostatic pressure forces, and the equal but opposite body force from resistive drag between the fluid and polymer. This form for the polymer dynamics is equivalent to assuming that the polymer is a Kelvin-Voigt material[20] with viscosity η_p. We choose this form because it qualitatively captures the effect of entanglements and crosslinks in a polymer network, and when $\mu = 0$, it describes an uncrosslinked polymer melt. Therefore,

$$\Gamma(\boldsymbol{v}_f - \boldsymbol{v}_p) = -(1-\phi)\nabla p + \eta_f \nabla \cdot (\nabla \boldsymbol{v}_f + \nabla \boldsymbol{v}_f^T) \,, \tag{2}$$

$$\Gamma(\boldsymbol{v}_p - \boldsymbol{v}_f) = -\phi \nabla p + \eta_p \nabla \cdot (\nabla \boldsymbol{v}_p + \nabla \boldsymbol{v}_p^T) + \frac{1}{\mathcal{J}} \nabla \cdot \left(\boldsymbol{S} \cdot \left(\boldsymbol{I} + (\nabla \boldsymbol{u})^T \right) \right) \,, \tag{3}$$

where η_f is the fluid viscosity and p is the hydrodynamic pressure. In these equations, the pressure force is distributed according to the volume fraction of the phase.[16] Resistive drag between the fluid and polymer is proportional to the velocity difference between the phases, where the drag coefficient Γ is the constant of proportionality. Scaling arguments suggest that Γ should be proportional to the viscosity of the fluid and inversely proportional to the average distance between the polymers. Using that the average distance between the polymers is approximately given by $2\pi a/\sqrt{\phi}$, where a is the radius of the polymer, we estimate that $\Gamma \sim \eta_f \phi / 4\pi^2 a^2$.

In Eq. (3), the elastic stress is written in terms of the second Piola-Kirchoff stress tensor $\boldsymbol{S}$, and the polymer displacement vector is $\boldsymbol{u}$. The gradient and divergence operators are all in terms of the lab coordinates, and $\boldsymbol{I}$ is the identity matrix. Here, $\mathcal{J}$ is the determinant of the deformation gradient tensor. In our simulations, we use the small deformation approximation and linear, isotropic elasticity to define the polymer stress tensor,

$$\boldsymbol{S} \cdot \left(\boldsymbol{I} + (\nabla \boldsymbol{u})^T \right) \approx \frac{\mu}{2} \left(\nabla \boldsymbol{u} + (\nabla \boldsymbol{u})^T \right) + \sigma_0 (\phi_0 - \phi) \boldsymbol{I} \,. \tag{4}$$

The elastic shear modulus is μ and the bulk modulus is σ_0. The unstressed volume fraction of the polymer is ϕ_0. It is straightforward to include the nonlinear terms in the strain tensor into our algorithm, but here, we ignore these terms for simplicity. The polymer displacement $\boldsymbol{u}$ is advected by the polymer velocity as

$$\frac{d\boldsymbol{u}}{dt} = \frac{\partial \boldsymbol{u}}{\partial t} + \boldsymbol{v}_p \cdot \nabla \boldsymbol{u} = \boldsymbol{v}_p \,. \tag{5}$$

Finally, conservation of volume demands that the divergence of the total flux is equal to zero:

$$\nabla \cdot \{(1-\phi)\boldsymbol{v}_f + \phi \boldsymbol{v}_p\} = 0 \,. \tag{6}$$

This article is copyrighted as indicated in the article. Reuse of AIP content is subject to the terms at: http://scitation.aip.org/termsconditions. Downloaded to IP: 128.196.189.33 On: Wed, 06 Jan 2016 19:05:57

Because we are using a continuum description where each volume element is considered to contain both fluid and polymer, this formulation assumes that the polymer diameter and inter-polymer spacing are small compared to the lengthscales of the immersed object (i.e., the swimmer). For cases where the inter-polymer spacing is comparable to or larger than the diameter of the immersed swimmer, it is necessary to treat the polymer as discrete objects, as has been done in Ref. 21.

III. THE IMMERSED BOUNDARY METHOD FOR TWO-PHASE FLUIDS

When an elastic sheet is immersed in a two-phase fluid, forces from the sheet are transmitted to each of the two phases. The fraction of the force that is transmitted to each phase is not given *a priori* but, rather, depends on the details of the interaction between the swimmer and the polymer. While the no-slip boundary condition requires that the fluid phase moves with the surface of the swimmer, polymers in the fluid can slip with respect to the surface of the swimmer. In fact, in dilute solutions, the polymer may not be in direct contact with the swimmer, as was pointed out in Ref. 22. We, therefore, assume that we can decompose the force from the sheet into a component that acts on the fluid, $\boldsymbol{F}_\mathrm{f}$, and a component that acts on the polymer, $\boldsymbol{F}_\mathrm{p}$. In the time-dependent Stokes equations (Eqs. (2) and (3)), these Lagrangian forces are spread onto the Eulerian domain as external forces,

$$\rho_\mathrm{f}\frac{\partial \boldsymbol{v}_\mathrm{f}}{\partial t} + \Gamma(\boldsymbol{v}_\mathrm{f} - \boldsymbol{v}_\mathrm{p}) = -(1-\phi)\nabla p + \eta_\mathrm{f}\nabla\cdot(\nabla\boldsymbol{v}_\mathrm{f} + \nabla\boldsymbol{v}_\mathrm{f}^\mathrm{T}) + S\boldsymbol{F}_\mathrm{f}\,, \tag{7}$$

$$\rho_\mathrm{p}\frac{\partial \boldsymbol{v}_\mathrm{p}}{\partial t} + \Gamma(\boldsymbol{v}_\mathrm{p} - \boldsymbol{v}_\mathrm{f}) = -\phi\nabla p - \sigma_0\nabla\phi + \eta_\mathrm{p}\nabla\cdot(\nabla\boldsymbol{v}_\mathrm{p} + \nabla\boldsymbol{v}_\mathrm{p}^\mathrm{T}) + \mu\nabla\cdot(\nabla\boldsymbol{u} + \nabla\boldsymbol{u}^\mathrm{T}) + S\boldsymbol{F}_\mathrm{p}. \tag{8}$$

Here, we have modified the two-phase force balance equations (Eqs. (7) and (8)) to include acceleration terms that are proportional to an effective density of each phase, i.e., we define ρ_f and ρ_p to be the effective densities of the fluid and polymer, respectively. In our simulations, we use the density of water for both phases, $\rho_\mathrm{f} = \rho_\mathrm{p} = 1$ g/ml. These inertial terms are included to provide additional stability to our algorithm and only negligibly affect the dynamics for low Reynolds number flows.[23] In addition, we define $S\boldsymbol{F}$, which is a function that spreads the Lagrangian forces onto the Eulerian domain, and $S^*\boldsymbol{v}$, which represents the interpolation of the velocity from the Eulerian domain to the Lagrangian structure. These functions can be written explicitly using the Dirac delta function,

$$S\boldsymbol{F}(\boldsymbol{x}) = \int_{\Omega_\mathrm{L}} \boldsymbol{F}(s)\delta(\boldsymbol{x} - \boldsymbol{X}(s))ds\,, \tag{9}$$

$$S^*\boldsymbol{u}(s) = \int_{\Omega_\mathrm{E}} \boldsymbol{u}(\boldsymbol{x})\delta(\boldsymbol{x} - \boldsymbol{X}(s))d\boldsymbol{x}\,, \tag{10}$$

where $\boldsymbol{X}(s)$ is the Lagrangian coordinate of the sheet in Ω_L and s is the arclength. The velocity of the sheet is determined by the no slip condition with the fluid phase,

$$\frac{\partial \boldsymbol{X}}{\partial t} = S^*\boldsymbol{v}_\mathrm{f}\,. \tag{11}$$

To compute the external force from the sheet on the polymer, we assume that the immersed sheet can slide with respect to the polymer and define drag coefficients Ξ_T and Ξ_N that define the tangential and normal components of the force, respectively, in terms of the velocity difference between the swimmer and the polymer (Eqs. (12) and (13)),

$$\boldsymbol{F}_\mathrm{p}\cdot\boldsymbol{T} = \Xi_\mathrm{T}S^*(\boldsymbol{v}_\mathrm{f} - \boldsymbol{v}_\mathrm{p})\cdot\boldsymbol{T}\,, \tag{12}$$

$$\boldsymbol{F}_\mathrm{p}\cdot\boldsymbol{N} = \Xi_\mathrm{N}S^*(\boldsymbol{v}_\mathrm{f} - \boldsymbol{v}_\mathrm{p})\cdot\boldsymbol{N}\,, \tag{13}$$

where $\boldsymbol{T}$ and $\boldsymbol{N}$ are the tangential and normal unit vectors of the sheet.

This article is copyrighted as indicated in the article. Reuse of AIP content is subject to the terms at: http://scitation.aip.org/termsconditions. Downloaded to IP: 128.196.189.33 On: Wed, 06 Jan 2016 19:05:57

The total force that is exerted by the sheet onto the fluid and polymer is equal to the functional derivative of the energy with respect to the centerline position of the sheet,

$$\boldsymbol{F}_{\mathrm{f}} + \boldsymbol{F}_{\mathrm{p}} = -\frac{\delta E}{\delta \boldsymbol{X}} \,. \tag{14}$$

As in Fu *et al.*,[22] we consider two types of boundary conditions between the immersed sheet and the swimmer, direct or solvent-mediated. The direct boundary condition describes contact between the sheet and polymer. The drag coefficients Ξ_{T} and Ξ_{N} are non-zero. If these drag coefficients are sufficiently large, then the polymer effectively does not slide with respect to the sheet. For example, when Ξ_{N} is large, the polymer moves with the sheet in the normal direction but can still slide in the tangential direction. In the solvent-mediated boundary condition, the interaction between the sheet and polymer is mediated by the fluid without direct contact between the sheet and polymer. Therefore, $\Xi_{\mathrm{T}} = \Xi_{\mathrm{N}} = 0$.

For the boundary conditions on the velocities of fluid and polymer, we apply periodic boundaries in both directions (x and y).

In our examples, we consider a sinusoidal-shaped swimmer that propagates traveling waves. The immersed boundary is an elastic sheet with stiffness coefficient K_{s}, bending modulus K_{b}, and undeformed shape defined by a spatial and temporally dependent preferred curvature $\kappa_0(s,t)$. The internal elastic energy E is then given by

$$E[\boldsymbol{X}(\cdot,t)] = \int_{\Omega_{\mathrm{L}}} \frac{1}{2} K_{\mathrm{s}} \left(\left| \frac{\partial \boldsymbol{X}}{\partial s} \right| - 1 \right)^2 + \frac{1}{2} K_{\mathrm{b}} \left| \frac{\partial^2 \boldsymbol{X}}{\partial s^2} \cdot \boldsymbol{N} - \kappa_0 \right|^2 ds \,. \tag{15}$$

We use an initial sheet configuration and reference traveling wave curvature given by

$$X(s) = (s, A \sin(ks)) \,, \tag{16}$$

$$\kappa_0 \;\; = -k^2 A \sin(ks - \omega t) \,, \tag{17}$$

where $k = 2\pi/\lambda$ is the wave number with wavelength λ, and ω is the undulation frequency. This definition of the preferred curvature is similar to what was used in Teran *et al.*[7]

IV. NUMERICAL METHODS

We solve the incompressible two-phase Stokes equations with the cell-centered approximate projection method.[24] The forces transmitted from the sheet to the polymer and the viscous terms are treated by the Crank-Nicolson method for the intermediate time steps and semi-implicitly for full time steps. We use a 2D computational domain with grid size h and Lagrangian parameter spacing Δs. The discrete gradient, divergence, and Laplacian operators G_h, $D_h\cdot$, and L_h, respectively, are discretized to the second order.[25] In our implementation, we use a Krylov subspace iterative method, such as the Generalized Minimal Residual Method (GMRES) in PETSc.[26]

We define the discretized operator for $\nabla \cdot (\nabla + \nabla^{\mathrm{T}})$ as follows:

$$\mathscr{L}_h = L_h + G_h D_h \cdot, \tag{18}$$

and the spreading operator S_n and the interpolation operator S_n^* by

$$(S_n \boldsymbol{F})_{i,j} = \sum_s \boldsymbol{F}_s \, \delta_h(\boldsymbol{x}_{i,j} - \boldsymbol{X}_s^n) \, \Delta s \,, \tag{19}$$

$$(S_n^* \boldsymbol{u})_s \;\; = \sum_{i,j} \boldsymbol{u}_{i,j} \, \delta_h(\boldsymbol{x}_{i,j} - \boldsymbol{X}_s^n) \, h^2 \,. \tag{20}$$

To construct δ_h, we use the four-point smoothed Dirac delta function $\phi(r)$ described by Peskin,[27]

$$\phi(r) = \begin{cases} 0, & |r| \geq 2, \\ \frac{1}{8}\left(5 - 2|r| - \sqrt{-7 + 12|r| - 4r^2}\right), & 2 \geq |r| \geq 1, \\ \frac{1}{8}\left(3 - 2|r| + \sqrt{1 + 4|r| - 4r^2}\right), & 1 \geq |r| \geq 0, \end{cases} \tag{21}$$

This article is copyrighted as indicated in the article. Reuse of AIP content is subject to the terms at: http://scitation.aip.org/termsconditions. Downloaded to IP: 128.196.189.33 On: Wed, 06 Jan 2016 19:05:57

where $r \in \mathrm{IR}$. The one-dimensional regularized Dirac delta function is then

$$\delta_h(x) = \frac{1}{h}\,\phi\left(\frac{x}{h}\right), \tag{22}$$

and the two-dimensional smoothed delta function is taken to be the tensor product of one-dimensional smoothed delta functions, i.e., $\delta_h(\mathbf{x}) = \delta_h(x_1)\,\delta_h(x_2)$, which is supported on the 4×4 grid box centered at the origin.

We take the following steps to solve the governing equations: At the beginning of a time step, the continuity equation for polymer volume fraction (1) is solved explicitly from ϕ^n to $\phi^{n+\frac{1}{2}}$,

$$\frac{\phi^{n+\frac{1}{2}} - \phi^n}{\Delta t/2} + D_h \cdot (\phi^n \boldsymbol{v}_\mathrm{p}^n) = 0\,, \tag{23}$$

and the solid displacement is updated from $\boldsymbol{u}^n$ to $\boldsymbol{u}^{n+\frac{1}{2}}$ using

$$\frac{\boldsymbol{u}^{n+\frac{1}{2}} - \boldsymbol{u}^n}{\Delta t/2} + \boldsymbol{v}_\mathrm{p}^n \cdot G_h \boldsymbol{u}^n = \boldsymbol{v}_\mathrm{p}^n. \tag{24}$$

We then compute the fluid and solid velocities, $\boldsymbol{v}_\mathrm{f}^*$ and $\boldsymbol{v}_\mathrm{p}^*$, at an intermediate time point but do not guarantee that the volume conservation condition is satisfied,

$$\begin{aligned}\rho_\mathrm{f}\frac{\boldsymbol{v}_\mathrm{f}^* - \boldsymbol{v}_\mathrm{f}^n}{\Delta t} + \Gamma(\boldsymbol{v}_\mathrm{f}^{n+\frac{1}{2},*} - \boldsymbol{v}_\mathrm{p}^{n+\frac{1}{2},*}) &= -(1-\phi^{n+\frac{1}{2}})G_h p^{n-\frac{1}{2}} \\ &\quad + \eta_\mathrm{f}\mathcal{L}_h \boldsymbol{v}_\mathrm{f}^{n+\frac{1}{2},*} + S_{n+\frac{1}{2}}\boldsymbol{F}_\mathrm{f}^{n+\frac{1}{2},*}\,, \end{aligned} \tag{25}$$

$$\begin{aligned}\rho_\mathrm{p}\frac{\boldsymbol{v}_\mathrm{p}^* - \boldsymbol{v}_\mathrm{p}^n}{\Delta t} + \Gamma(\boldsymbol{v}_\mathrm{p}^{n+\frac{1}{2},*} - \boldsymbol{v}_\mathrm{f}^{n+\frac{1}{2},*}) &= -\phi^{n+\frac{1}{2}}G_h p^{n-\frac{1}{2}} - \sigma_0 G_h \phi^{n+\frac{1}{2}} \\ &\quad + \eta_\mathrm{p}\mathcal{L}_h \boldsymbol{v}_\mathrm{p}^{n+\frac{1}{2},*} + \mu\mathcal{L}_h \boldsymbol{u}^{n+\frac{1}{2}} + S_{n+\frac{1}{2}}\boldsymbol{F}_\mathrm{p}^{n+\frac{1}{2},*}, \end{aligned} \tag{26}$$

with the velocities and the sheet position at the half-time step defined as

$$\boldsymbol{v}_\mathrm{f}^{n+\frac{1}{2},*} = \frac{\boldsymbol{v}_\mathrm{f}^n + \boldsymbol{v}_\mathrm{f}^*}{2}, \qquad \boldsymbol{v}_\mathrm{p}^{n+\frac{1}{2},*} = \frac{\boldsymbol{v}_\mathrm{p}^n + \boldsymbol{v}_\mathrm{p}^*}{2}, \tag{27}$$

$$\frac{\boldsymbol{X}^{n+\frac{1}{2}} - \boldsymbol{X}^n}{\Delta t/2} = S_n^* \boldsymbol{v}_\mathrm{f}^n, \tag{28}$$

where the forces transmitted from the sheet to the polymer are explicitly discretized as

$$\begin{aligned}\boldsymbol{F}_\mathrm{p}^{n+\frac{1}{2},*} &= \Xi_\mathrm{T}(\boldsymbol{v}_\mathrm{f}^{n+\frac{1}{2},*} - \boldsymbol{v}_\mathrm{p}^{n+\frac{1}{2},*}) \cdot \boldsymbol{T}^{n+\frac{1}{2}}\boldsymbol{T}^{n+\frac{1}{2}} \\ &\quad + \Xi_\mathrm{N}(\boldsymbol{v}_\mathrm{f}^{n+\frac{1}{2},*} - \boldsymbol{v}_\mathrm{p}^{n+\frac{1}{2},*}) \cdot \boldsymbol{N}^{n+\frac{1}{2}}\boldsymbol{N}^{n+\frac{1}{2}}\,, \end{aligned} \tag{29}$$

$$\boldsymbol{F}_\mathrm{f}^{n+\frac{1}{2},*} = -\frac{\partial E}{\partial \boldsymbol{X}^{n+\frac{1}{2}}} - \boldsymbol{F}_\mathrm{p}^{n+\frac{1}{2},*}\,. \tag{30}$$

Next, with the approximate projection method, we solve for the velocities $\boldsymbol{v}_\mathrm{f}^{n+1}$ and $\boldsymbol{v}_\mathrm{p}^{n+1}$, so as to impose volume conservation,

$$\begin{aligned}\rho_\mathrm{f}\frac{\boldsymbol{v}_\mathrm{f}^{n+1} - \boldsymbol{v}_\mathrm{f}^n}{\Delta t} + \Gamma(\boldsymbol{v}_\mathrm{f}^{n+\frac{1}{2}} - \boldsymbol{v}_\mathrm{p}^{n+\frac{1}{2}}) &= -(1-\phi^{n+\frac{1}{2}})G_h p^{n+\frac{1}{2}} \\ &\quad + \eta_\mathrm{f}\mathcal{L}_h \boldsymbol{v}_\mathrm{f}^{n+1} + S_{n+\frac{1}{2}}\boldsymbol{F}_\mathrm{f}^{n+1}\,, \end{aligned} \tag{31}$$

$$\begin{aligned}\rho_\mathrm{p}\frac{\boldsymbol{v}_\mathrm{p}^{n+1} - \boldsymbol{v}_\mathrm{p}^n}{\Delta t} + \Gamma(\boldsymbol{v}_\mathrm{p}^{n+\frac{1}{2}} - \boldsymbol{v}_\mathrm{f}^{n+\frac{1}{2}}) &= -\phi^{n+\frac{1}{2}}G_h p^{n+\frac{1}{2}} - \sigma_0 G_h \phi^{n+\frac{1}{2}} \\ &\quad + \eta_\mathrm{p}\mathcal{L}_h \boldsymbol{v}_\mathrm{p}^{n+1} + \mu\mathcal{L}_h \boldsymbol{u}^{n+\frac{1}{2}} + S_{n+\frac{1}{2}}\boldsymbol{F}_\mathrm{p}^{n+1}\,, \end{aligned} \tag{32}$$

This article is copyrighted as indicated in the article. Reuse of AIP content is subject to the terms at: http://scitation.aip.org/termsconditions. Downloaded to IP: 128.196.189.33 On: Wed, 06 Jan 2016 19:05:57

with the velocities and the sheet position at the half-time step defined as

$$\boldsymbol{v}_{\mathrm{f}}^{n+\frac{1}{2}} = \frac{\boldsymbol{v}_{\mathrm{f}}^{n} + \boldsymbol{v}_{\mathrm{f}}^{n+1}}{2}, \qquad \boldsymbol{v}_{\mathrm{p}}^{n+\frac{1}{2}} = \frac{\boldsymbol{v}_{\mathrm{p}}^{n} + \boldsymbol{v}_{\mathrm{p}}^{n+1}}{2}, \tag{33}$$

where the forces transmitted from the sheet to the polymer are computed semi-implicitly,

$$\begin{aligned}\boldsymbol{F}_{\mathrm{p}}^{n+1} &= \Xi_{\mathrm{T}}(\boldsymbol{v}_{\mathrm{f}}^{n+1} - \boldsymbol{v}_{\mathrm{p}}^{n+1}) \cdot \boldsymbol{T}^{n+\frac{1}{2}}\boldsymbol{T}^{n+\frac{1}{2}} \\ &\quad + \Xi_{\mathrm{N}}(\boldsymbol{v}_{\mathrm{f}}^{n+1} - \boldsymbol{v}_{\mathrm{p}}^{n+1}) \cdot \boldsymbol{N}^{n+\frac{1}{2}}\boldsymbol{N}^{n+\frac{1}{2}}\,,\end{aligned} \tag{34}$$

$$\boldsymbol{F}_{\mathrm{f}}^{n+1} = -\frac{\partial E}{\partial \boldsymbol{X}^{n+\frac{1}{2}}} - \boldsymbol{F}_{\mathrm{p}}^{n+1}\,. \tag{35}$$

After algebraic rearrangement, we solve the following linear system:

$$\begin{pmatrix} m_{\mathrm{f}} & m_{\mathrm{p}} \\ 1-\phi^{n+1} & \phi^{n+1} \end{pmatrix} \begin{pmatrix} \boldsymbol{v}_{\mathrm{f}}^{n+1} \\ \boldsymbol{v}_{\mathrm{p}}^{n+1} \end{pmatrix} = \begin{pmatrix} r_{\mathrm{f}} \\ r_{\mathrm{p}} \end{pmatrix}, \tag{36}$$

where

$$\begin{aligned}
m_{\mathrm{f}} &= \frac{\phi^{n+\frac{1}{2}}\rho_{\mathrm{f}}}{\Delta t} + \frac{\Gamma}{2} - \phi^{n+\frac{1}{2}}\eta_{\mathrm{f}}\mathcal{L}_h + \Xi_{\mathrm{T}}\mathcal{P}_{\mathrm{T}}^{n+\frac{1}{2}} + \Xi_{\mathrm{N}}\mathcal{P}_{\mathrm{N}}^{n+\frac{1}{2}}\,,\\
m_{\mathrm{p}} &= -\frac{(1-\phi^{n+\frac{1}{2}})\rho_{\mathrm{p}}}{\Delta t} - \frac{\Gamma}{2} + (1-\phi^{n+\frac{1}{2}})\eta_{\mathrm{p}}\mathcal{L}_h - \Xi_{\mathrm{T}}\mathcal{P}_{\mathrm{T}}^{n+\frac{1}{2}} - \Xi_{\mathrm{N}}\mathcal{P}_{\mathrm{N}}^{n+\frac{1}{2}}\,,\\
r_{\mathrm{f}} &= (\frac{\phi^{n+\frac{1}{2}}\rho_{\mathrm{f}}}{\Delta t} - \frac{\Gamma}{2} + \phi^{n+\frac{1}{2}}\eta_{\mathrm{f}}\mathcal{L}_h)\boldsymbol{v}_{\mathrm{f}}^{n} + (-\frac{(1-\phi^{n+\frac{1}{2}})\rho_{\mathrm{p}}}{\Delta t} + \frac{\Gamma}{2} - (1-\phi^{n+\frac{1}{2}})\eta_{\mathrm{p}}\mathcal{L}_h)\boldsymbol{v}_{\mathrm{p}}^{n}\\
&\quad -\phi^{n+\frac{1}{2}}S_{n+\frac{1}{2}}\frac{\delta E}{\delta \boldsymbol{X}^{n+\frac{1}{2}}} - (1-\phi^{n+\frac{1}{2}})\mu\mathcal{L}_h\boldsymbol{u}^{n+\frac{1}{2}} + \sigma_0(1-\phi^{n+\frac{1}{2}})G_h\phi^{n+\frac{1}{2}}\,,\\
r_{\mathrm{p}} &= \mathcal{P}\{(1-\phi^{n+1})\boldsymbol{v}_{\mathrm{f}}^{*} + \phi^{n+1}\boldsymbol{v}_{\mathrm{p}}^{*}\}\,,
\end{aligned}$$

and the approximate projection operator $\mathcal{P}$ is

$$\mathcal{P} = I - G_h L_h^{-1} D_h\cdot \tag{37}$$

The tangential and normal projection operators $\mathcal{P}_{\mathrm{T}}$ and $\mathcal{P}_{\mathrm{N}}$ are

$$\mathcal{P}_{\mathrm{T}}^{n}(\boldsymbol{v}) = S_n(S_n^{*}\boldsymbol{v}\cdot\boldsymbol{T}^{n}\boldsymbol{T}^{n})\,, \tag{38}$$

$$\mathcal{P}_{\mathrm{N}}^{n}(\boldsymbol{v}) = S_n(S_n^{*}\boldsymbol{v}\cdot\boldsymbol{N}^{n}\boldsymbol{N}^{n})\,. \tag{39}$$

The hydrodynamic pressure is then updated from $p^{n-\frac{1}{2}}$ to $p^{n+\frac{1}{2}}$ using

$$\begin{aligned}p^{n+\frac{1}{2}} - p^{n-\frac{1}{2}} &= L_h^{-1}D_h\cdot\{\rho_{\mathrm{f}}\frac{\boldsymbol{v}_{\mathrm{f}}^{*} - \boldsymbol{v}_{\mathrm{f}}^{n+1}}{\Delta t} + \rho_{\mathrm{p}}\frac{\boldsymbol{v}_{\mathrm{p}}^{*} - \boldsymbol{v}_{\mathrm{p}}^{n+1}}{\Delta t}\\ &\quad + \eta_{\mathrm{f}}\mathcal{L}_h(\boldsymbol{v}_{\mathrm{f}}^{n+1} - \boldsymbol{v}_{\mathrm{f}}^{n+\frac{1}{2},*}) + \eta_{\mathrm{p}}\mathcal{L}_h(\boldsymbol{v}_{\mathrm{p}}^{n+1} - \boldsymbol{v}_{\mathrm{p}}^{n+\frac{1}{2},*})\},\end{aligned} \tag{40}$$

and the sheet position is updated from $\boldsymbol{X}^{n}$ to $\boldsymbol{X}^{n+1}$ using the no slip condition,

$$\frac{\boldsymbol{X}^{n+1} - \boldsymbol{X}^{n}}{\Delta t} = S_n^{*}\boldsymbol{v}_{\mathrm{f}}^{n+\frac{1}{2}}\,. \tag{41}$$

Finally, the polymer volume fraction and solid displacement are updated to ϕ^{n+1} and $\boldsymbol{u}^{n+1}$,

$$\frac{\phi^{n+1} - \phi^{n}}{\Delta t} + D_h\cdot(\phi^{n+\frac{1}{2}}\boldsymbol{v}_{\mathrm{p}}^{n+\frac{1}{2}}) = 0, \tag{42}$$

$$\frac{\boldsymbol{u}^{n+1} - \boldsymbol{u}^{n}}{\Delta t} + \boldsymbol{v}_{\mathrm{p}}^{n+\frac{1}{2}}\cdot G_h\boldsymbol{u}^{n+\frac{1}{2}} = \boldsymbol{v}_{\mathrm{p}}^{n+\frac{1}{2}}. \tag{43}$$

This article is copyrighted as indicated in the article. Reuse of AIP content is subject to the terms at: http://scitation.aip.org/termsconditions. Downloaded to IP: 128.196.189.33 On: Wed, 06 Jan 2016 19:05:57

The discretization of the variational derivative of the bending energy functional gives components of the force per length at the ith node of Fauci and Peskin,[28]

$$F_{x,i} = \frac{K_b}{\Delta s^2}\left((\kappa-\kappa_0)_{i-1}(Y_{i-1}-Y_{i-2}) - (\kappa-\kappa_0)_i(Y_{i+1}-Y_{i-1}) + (\kappa-\kappa_0)_{i+1}(Y_{i+2}-Y_{i+1})\right), \tag{44}$$

$$F_{y,i} = -\frac{K_b}{\Delta s^2}\left((\kappa-\kappa_0)_{i-1}(X_{i-1}-X_{i-2}) - (\kappa-\kappa_0)_i(X_{i+1}-X_{i-1}) + (\kappa-\kappa_0)_{i+1}(X_{i+2}-X_{i+1})\right), \tag{45}$$

where $\kappa_i = \boldsymbol{z}\cdot(\boldsymbol{X}_{i+1}-\boldsymbol{X}_i)\times(\boldsymbol{X}_i-\boldsymbol{X}_{i-1})/\Delta s^3$.

V. NUMERICAL RESULTS

In order to show that our two-phase immersed boundary method provides a robust way for simulating fluid-structure interactions in a general composite fluid composed of polymer and fluid, we need to show that our algorithm can reproduce theoretical results for swimming in viscoelastic fluids (which represent a polymer melt where the polymer is not crosslinked) and gels (where a connected polymer network is immersed in a viscous fluid). The theories that have been done to date typically consider a sinusoidally oscillating sheet or sheet in a complex fluid. Therefore, we consider an oscillating sheet in a 2D two-phase fluid.

In our simulations, the computational domain is 50 μm × 50 μm with 256 nodes in each direction and it takes approximately 12 h to compute one swimming cycle. The swimming sheet has an initial configuration and reference curvature defined by Eqs. (16) and (17) with amplitude $A = 0.25$ μm, wavelength $\lambda = 5$ μm, and an undulation frequency $\omega = 5$ Hz. We use a tensile stiffness $K_s = 2.048\times10^{-8}$ N/m, which is selected to maintain the sheet length to within 2.5%. The bending modulus K_b is 6.0×10^{-12} N m, and we assume that the fluid phase has the density and viscosity of water. We compute the average swimming velocity over the whole timespan T as

$$v = \frac{1}{T}\int_0^T \boldsymbol{v}_c(t)\cdot\boldsymbol{d}_G(t)dt, \tag{46}$$

where $\boldsymbol{v}_c(t)$ and $\boldsymbol{d}_G(t)$ are the instantaneous velocity of the center and the directional unit vector of the sheet (i.e., a unit vector in the direction of the line that connects the end points of the swimmer at time t), respectively.

In Figure 1 (Multimedia view), we compare two swimmers, one in a Newtonian fluid (dashed curve) and the other in a 2% polymer solution with a direct boundary condition with $\Xi_T = 32$ Pa s

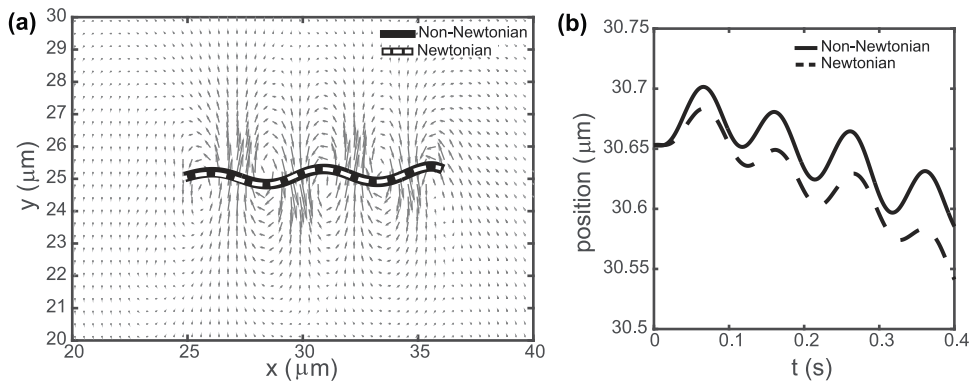

FIG. 1. Snapshot of a swimmer in a non-Newtonian fluid at time 0.4 s (a) and the trajectory of the centroid (b). The solid curve shows the shape of the swimmer, and the light gray arrows show the flow field for the non-Newtonian fluid. Corresponding shape and position of a swimmer in a Newtonian fluid are shown with a dashed white curve. (Multimedia view) [URL: http://dx.doi.org/10.1063/1.4938174.1][URL: http://dx.doi.org/10.1063/1.4938174.2]

This article is copyrighted as indicated in the article. Reuse of AIP content is subject to the terms at: http://scitation.aip.org/termsconditions. Downloaded to IP: 128.196.189.33 On: Wed, 06 Jan 2016 19:05:57

and Ξ_N = 100 Pa s (solid curve). The fluid velocity field and the configuration of the sheet during the course of swimming are shown for the two-phase medium. Snapshot shows time t = 0.4 s. In this simulation, the fluid-polymer drag coefficient is $\Gamma = 1.7844 \times 10^9$ Pa s/m^2 and the polymer viscosity is the same as the fluid viscosity. The elastic shear modulus μ is 3.5×10^{-3} Pa. In this simulation, we find that the swimming pattern is similar to the Newtonian case; however, the two-phase medium reduces the swimming speed. A movie that shows simultaneously the motion of the swimmer in the Newtonian and non-Newtonian fluids is included (see Figure 1 (Multimedia view)).

As a first test of our algorithm, we compared our results to the analytical work in Fu *et al.*,[22] who considered the swimming of a small amplitude, infinite sheet in a 2D gel composed of a viscous fluid and a linearly elastic polymer network. Our framework allows a direct comparison with this theoretical result by setting the polymer viscosity to zero. Fu *et al.*[22] computed the swimming speed of the undulating swimmer for a large number of cases. We explored a few of these using a preferred curvature (Eq. (17)) that defines a traveling wave swimmer with amplitude 0.5 μm and wavelength of 50 μm. To implement the infinite length swimmer in our numerics, we used a 50 μm $\times$ 50 μm periodic domain with the first and last Lagrangian nodes for the swimmer connected to each other. We examined how the velocity of the swimmer was affected by the dimensionless ratio of the fluid viscosity times the wave number divided by the tangential drag coefficient between the swimmer and polymer, $\eta_f k/\Xi_T$. We used the direct boundary condition with a large value of $\Xi_N = 1.0 \times 10^3$ Pa s to constrain the normal component of the polymer motion to move with the swimmer. Our results of large amplitude and finite length show some deviations from Fig. 2 of Fu *et al.*,[22] for both a compliant polymer network and an incompressible network, as is shown in Fig. 2(a) (the polymer networks are called compliant and incompressible when $\eta_f\omega/\mu$ and the bulk modulus σ_0 are sufficiently large, respectively). We hypothesized that the deviations were due to the fact that we were considering a moderate-sized undulation amplitude of a finite-length swimmer. We, therefore, simulated the swimming of an infinite sheet with small amplitude undulations. These simulations gave normalized velocities that were within 17% of the analytical theory (Figure 2(a)). We then tested our algorithm for the solvent-mediated boundary condition by examining the swimming speed as a function of the dimensionless parameter $\Gamma/\eta_f k^2$. For this test case, our simulations agree quite well (within 20%) with the Fu *et al.* results[22] whether the swimmer is finite-length and large amplitude or infinite-length and small amplitude.

We used the small amplitude, infinite length swimmer with the solvent-mediated boundary condition as a test case for the convergence of our algorithm. We ran the same simulations that

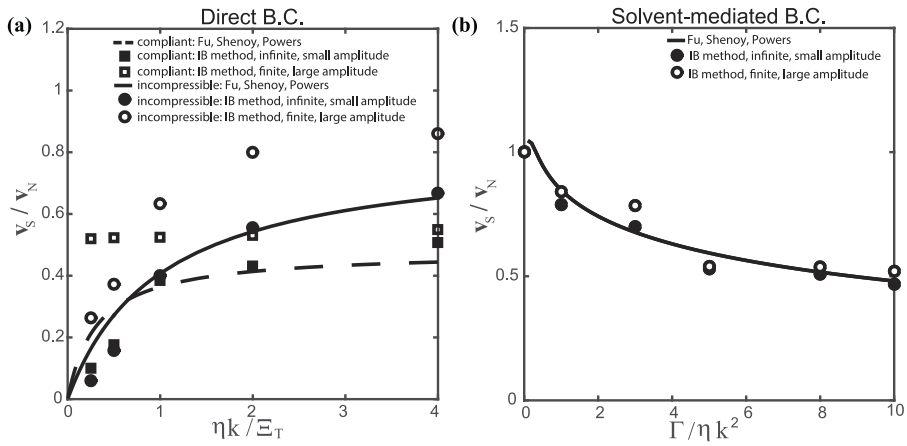

FIG. 2. Normalized swimming speed computed using the two-phase IB simulations compared to the results from Fu *et al.*[22] (a) Comparison of the direct boundary condition with Figure 2 in Ref. 22. For the incompressible case, $\sigma_0 = 5$ kPa and $\Gamma/(\eta_f k^2) = 1$; for the compliant case, $\eta_f\omega/\mu = 10$, $\sigma_0 = \mu, \Gamma/(\eta k^2) = 10$. The elastic modulus η is set to 0.0035 Pa. (b) Comparison of the solvent-mediated boundary condition with Figure 5 in Fu *et al.*[22] These simulations use $\eta_p = 0$, $\sigma_0 = 0$, and $\eta_f\omega/\mu = 10$. Results shown are from simulations on a 256×256 grid.

This article is copyrighted as indicated in the article. Reuse of AIP content is subject to the terms at: http://scitation.aip.org/termsconditions. Downloaded to IP: 128.196.189.33 On: Wed, 06 Jan 2016 19:05:57

were done for Figure 2(b) using four grids of size 32, 64, 128, and 256 and a time step that was proportional to the square of the grid spacing. The results were compared after one cycle of the swimmer's motion. We computed the L_2 norm of the error for the fluid and polymer velocities and the pressure and found that the convergence rate was 1.73 for the fluid and polymer velocities, and 1.70 for the pressure. We also computed the error between the swimming speed computed using the small amplitude swimmer and the analytical results from Fu *et al.*[22] The percent error in the swimming speed converged from 8.8% on the 64×64 grid to 5.1% on the 256×256 grid. For the large amplitude swimmer, we computed the relative difference in the calculated velocities for successively smaller grids. We found that the difference between the 64×64 grid and the 256×256 grid was 5.6%, whereas the difference between the 128×128 grid and the 256×256 grid was 2.6%. Therefore, our algorithm gives an approximately first order convergence in the velocity with grid spacing and over all the errors computed is between first and second order accurate.

Previous work by Lauga showed that for a wide range of single phase viscoelastic fluid models (e.g., Oldroyd B, Upper Convected Maxwell, and FENE-P) that increases in the Deborah number lead to decreases in the swimming speed of an undulating, small amplitude sheet.[6] An interesting aspect of this work was that the swimming speed did not depend on which viscoelastic fluid model was chosen; the speed was only a function of the Deborah number. As many of these single phase viscoelastic fluid models are meant to approximate the behavior of multi-component fluids, we sought to determine whether our two-phase simulations would produce similar results for the swimming speed in regimes that have similar physical characteristics as those of the single phase models. One major assumption of the single phase fluid models is that they treat polymer and fluid in the environment using a single velocity with a single boundary condition at the surface of the swimmer. Therefore, we simulated an immersed, undulating sheet and used the direct boundary condition to impose a no-slip condition for the force balance on both phases. In addition, we used the solvent-mediated boundary condition to mimic the case where only the fluid is in contact with the swimmer. Because the single phase models that Lauga considered do not have a finite elastic modulus at zero frequency, we set the elastic shear modulus $\mu = 0$. A second difficulty with comparing to the Lauga results is that our two-phase model does not have an explicit relaxation time with which to define the Deborah number. However, the Deborah number describes the relaxation of the stress in the medium with respect to the undulation frequency of the swimmer. In our two-phase model, the stress in the medium relaxes due to motion between the polymer phase and the fluid. The relaxation time is therefore dependent on the elastic modulus of the gel and the drag between the fluid and polymer. One can then define a pseudo-Deborah number for the two-phase system from the balance of polymer stress with the dissipative forces in the fluid and polymer. In our simulations, the polymer-fluid drag coefficient is large compared to the shear viscosities in either phases. Therefore, we use the polymer-fluid drag coefficient as a measure of the dissipative forces. The pseudo-Deborah number is then $De_{\mathrm{p}} = 15\Gamma\omega/\sigma_0\phi_0 k^2$, where the factor of 15 is determined empirically. The normalized swimming velocity (the ratio between non-Newtonian and Newtonian swimming velocity $v_{\mathrm{S}}/v_{\mathrm{N}}$) versus De_{p} can then be compared with the formula of Lauga,[6]

$$v_{\mathrm{S}}/v_{\mathrm{N}} = \frac{1 + \eta_{\mathrm{f}}/\eta De^2}{1 + De^2}\,, \tag{47}$$

where $\eta = \eta_{\mathrm{f}} + \eta_{\mathrm{p}}$. Figure 3 shows that the solvent-mediated boundary conditions agree quite well with Eq. (47); however, the direct boundary conditions produce slower swimming speeds (square points). However, a major difference between our two-phase model and the single phase descriptions used in Lauga is that the two-phase model includes an isotropic stress that is proportional to the polymer density. This stress behaves viscoelastically if the polymer can relax, but behaves elastically if the polymer is prevented from relaxing. The solvent-mediated boundary condition allows the polymer to slide past the swimmer in the transverse direction, whereas the direct boundary condition does not. Therefore, the solvent-mediated boundary condition may be a better analogue to the single-phase visco-elastic fluid models. As was seen with our comparison to Fu *et al.*,[22] the analytic solution and numerical solutions agree well when a small amplitude, infinite length swimmer is considered; however, the finite length swimmer shows some moderate deviations with the analytic expression for the normalized speed. Another factor that may be leading to some of the

This article is copyrighted as indicated in the article. Reuse of AIP content is subject to the terms at: http://scitation.aip.org/termsconditions. Downloaded to IP: 128.196.189.33 On: Wed, 06 Jan 2016 19:05:57

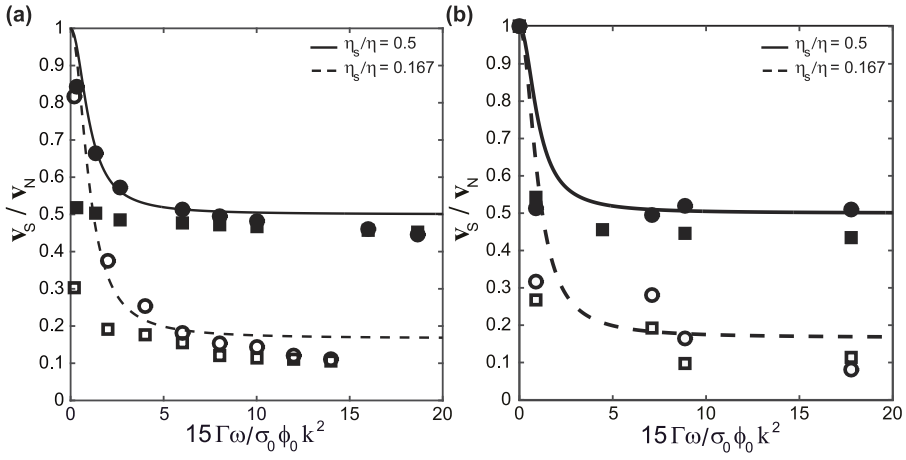

FIG. 3. Normalized velocity versus pseudo-Deborah number as compared with Eq. (47) for a viscoelastic fluid with $\mu = 0$. The solid and dotted curves show the analytic result for $\eta_S/\eta = 0.5$ and 0.167, respectively. The two-phase IB results are shown for the solvent-mediated boundary condition (round points) and the direct boundary condition (squares) with $\Xi_T/\Xi_N = 10^{-2}$. The IB solution with $\eta_S/\eta = 0.5$ (filled) and 0.167 (unfilled) are shown for a small amplitude, infinite swimmer (a) and for a finite length swimmer (b).

discrepancy between our simulations and Lauga's results is that the two-phase model does not have explicit shear stress relaxation. Therefore, our definition of an effective Deborah number does not fully capture the single-phase dynamic model that was previously investigated.

Next, we consider a more general case, where the polymer contributes elasticity and viscosity. Here, we examine how the swimming speed depends on the polymer volume fraction, the tangential drag coefficient, and the polymer viscosity. As shown in Figure 4, the polymer volume fraction only has a modest effect on the swimming speed, and, for the parameters that we examined, the tangential drag coefficient only affects swimming speed at small volume fraction (Figure 4(b)). However, the polymer viscosity has a substantial effect on swimming speed, with increasing viscosity leading to a decrease in swimming speed (Figure 4(a)).

VI. SIMULATING THE SWIMMING OF *C. elegans* THROUGH VISCOELASTIC FLUIDS

While the agreement between our numerical results and previously published analytic theories provides good evidence that our algorithm provides an accurate method for simulating the

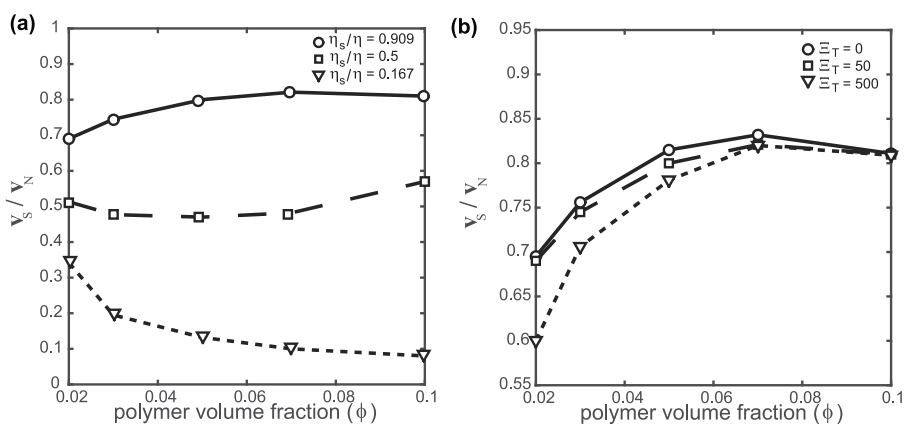

FIG. 4. (a) The normalized swimming velocity v_S/v_N versus ϕ for three different values of the normalized viscosity $\eta_S/\eta = 0.909$ (solid), 0.5 (dashed), and 0.167 (dotted). $\Xi_T/\Xi_N = 10^{-2}$. (b) v_S/v_N versus the polymer volume fraction ϕ for three different values of the normalized tangential drag coefficient, $\Xi_T/\Xi_N = 0$ (solid), 10^{-2} (dashed), and 10^{-1} (dotted). $\eta_S/\eta = 0.909$.

This article is copyrighted as indicated in the article. Reuse of AIP content is subject to the terms at: http://scitation.aip.org/termsconditions. Downloaded to IP: 128.196.189.33 On: Wed, 06 Jan 2016 19:05:57

interaction between a thin, elastic swimmer and a general non-Newtonian fluid, it remains unclear whether any of the theories and/or simulations of swimming through non-Newtonian fluids capture the actual physics of a real swimmer moving through a complex fluid environment. To begin to address this problem, we consider the swimming of the nematode *C. elegans* moving through a viscoelastic fluid. We chose this system because recent experiments have measured quantitatively the kinematics and swimming speed of *C. elegans* through viscous and viscoelastic fluids. *C. elegans* swims through viscous fluids by undulating its body as a roughly planar traveling wave with a wavelength of 1.5 and a mean curvature of approximately 3 in units normalized to the length of the worm.[4] The wavelength and mean curvature change only moderately (<50%) as the viscosity is increased from 1 to 100 mPa s; however, the wave speed of the traveling undulation decreases by roughly a factor of two over this same range.[8] When the nematode swims through a viscoelastic fluid composed of low concentrations of carboxymethyl cellulose, the wave speed is the same as in a purely viscous fluid with the same viscosity; viscoelasticity of the medium, though, reduces the swimming speed.[8] The slowing of *C. elegans* in viscoelastic media may be due to hyperbolic points in the fluid flow that occur away from the body of the swimmer, which can extend the polymers in these regions.[8]

In order to explore whether our two-phase IB method can reproduce the behaviors observed in Shen and Arratia,[8] we simulated the swimming of *C. elegans* through viscous and viscoelastic fluids using the kinematic data measured in Refs. 4 and 8, i.e., we used a body length 1.0 mm, the amplitude of the undulation A is 0.26 mm, and the wavelength λ is 2.5 mm. The elasticity of the swimmer was set to $K_s = 3.6 \times 10^{-5}$ N/m and $K_b = 4.91 \times 10^{-8}$ N m. We obtained the rheological data from Arratia's group in order to set the values of the polymer viscosity and Deborah number in our two-phase model as a function of the volume fraction (Table I). The effective viscosity that is measured should be equal to the sum of the fluid and polymer viscosities. Since the fluid viscosity is that of water, we can set the polymer viscosity as the measured viscosity minus the viscosity of water. We assume that our definition of the effective Deborah number, $De_p = 15\Gamma\omega/\sigma_0\phi_0 k^2$, should be roughly equivalent to the measured Deborah number. At low polymer densities, the polymer should behave similar to an ideal gas. Therefore, $\sigma_0 = k_B T/V$, where $k_B T$ is thermal energy and V is the volume of a single polymer,[29] which allows us to estimate that $\sigma_0 \approx 500$ Pa. The experimentally measured Deborah number can then be used to set Γ. These values for the parameters place the two-phase fluid model in the complex flow regime.

We ran simulations on a 5 mm × 5 mm domain and computed the average swimming speed. In Figure 5(a), we show how the swimming speed varied as a function of viscosity in Newtonian and non-Newtonian environments and compare our simulation results to the experimental measurements from Shen and Arratia.[8] The fact that our simulations for swimming through a viscous fluid are in good agreement with the experimental measurements is not surprising since the kinematic motions have been measured. Using these same kinematic parameters, we also find good agreement with the swimming speed for movement through viscoelastic media. To further compare our results to the experimental measurements, we also computed the normalized swimming speed (i.e., the ratio of the swimming speed in the viscoelastic medium to the speed in a viscous fluid with the same viscosity) as a function of the effective Deborah number described previously. Here, too, we find good agreement between our results and the experimental measurements (Figure 5(b)). We find

TABLE I. The viscosity and Deborah number as a function of polymer volume fraction for the experiments in Shen and Arratia.[8] Data courtesy of Arratia.

Volume fraction, ϕ_0 (%)	Deborah number, De	Viscosity, μ (mPa s)
0.146	1.02	48.0
0.195	0.83	66.7
0.486	2.95	241.8
0.584	4.12	381.5
0.778	5.13	678.0

This article is copyrighted as indicated in the article. Reuse of AIP content is subject to the terms at: http://scitation.aip.org/termsconditions. Downloaded to IP: 128.196.189.33 On: Wed, 06 Jan 2016 19:05:57

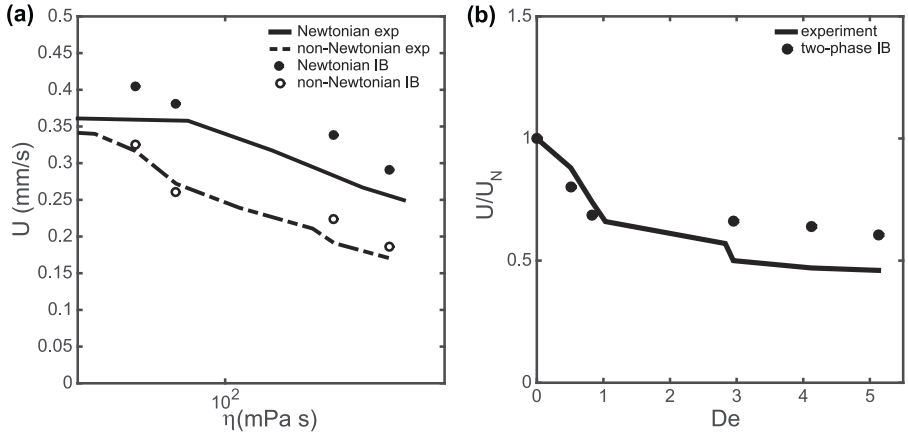

FIG. 5. Comparison of the two-phase IB to experiments on the swimming of *C. elegans*.[8] (a) Numerical results for the swimming of *C. elegans* through Newtonian (filled circles) and viscoelastic (open circles) fluids as a function of viscosity with a comparison to the experimental results (Newtonian fluid (solid curve), viscoelastic fluid (dotted curve)). (b) Normalized swimming speed versus Deborah number for the two-phase IB (open circles) and experiments (solid curve). These simulations were performed on a 128×128 grid.

that a decrease in speed with increasing Deborah number is likely a consequence of the fact that the estimated bending modulus for *C. elegans* is large enough that viscoelasticity in the environment does not alter the kinematics of *C. elegans*. Recently, Thomases and Guy[30] showed by simulating a swimmer moving through an Oldroyd B fluid that stiff swimmers are slowed by viscoelastic fluids.

As a final comparison, we investigated the fluid flow profiles about the swimmer for the Newtonian and non-Newtonian fluid environments. As previously mentioned, in experiments, Shen and Arratia[8] observed hyperbolic points in the viscoelastic media that were located away from the body of the swimmer, whereas in Newtonian fluids, hyperbolic points are only observed near the swimmer's body. From our simulations, we observe the same behavior. In a Newtonian fluid, hyperbolic points in the frame of the swimmer are only observed immediately adjacent to the body of the swimmer, while a hyperbolic point is observed "within the flow" (i.e., over half a body length away from the nematode's body) in simulations for the viscoelastic fluid (Figure 6). It should be noted that the definition of "near the body" and "within the flow" is defined somewhat qualitatively; however, for both of these cases, the streamlines of the flow in our simulations appear similar to what is observed experimentally. In addition, in order to clarify the physical advent of these hyperbolic points, we examined the magnitude of the elastic component of the stress tensor, similar to what

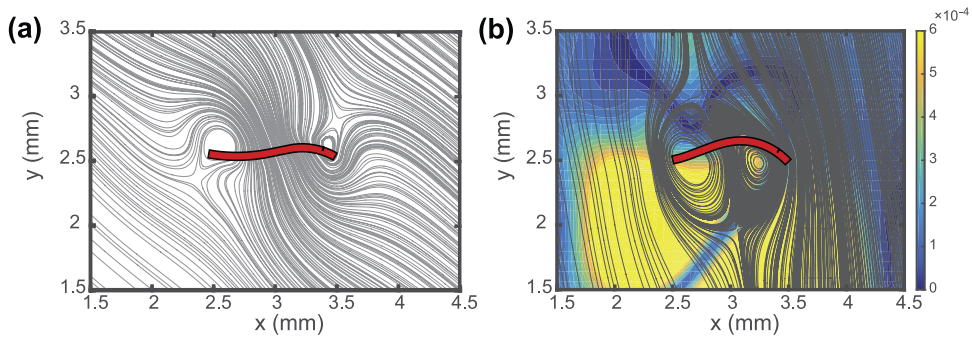

FIG. 6. Flow streamlines about a swimming *C. elegans*. Streamlines (gray) in the frame of the swimmer at time $t = 0.38$ s for a swimmer in the Newtonian (a) and non-Newtonian (b) environments are shown. The shape of the swimmer at time $t = 0.38$ s (solid curve) is also shown. The colormap shows the magnitude of the trace of the elastic stress, which is largest near the hyperbolic point that is observed away from the swimmer in the viscoelastic medium.

This article is copyrighted as indicated in the article. Reuse of AIP content is subject to the terms at: http://scitation.aip.org/termsconditions. Downloaded to IP: 128.196.189.33 On: Wed, 06 Jan 2016 19:05:57

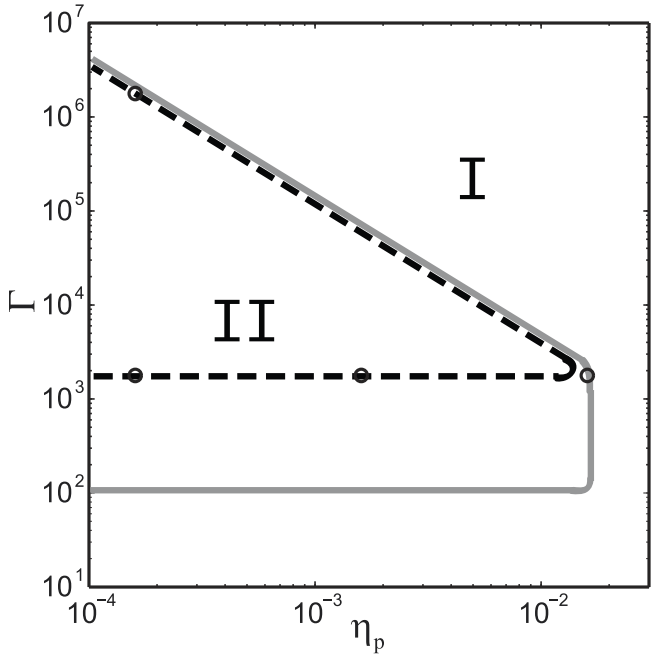

FIG. 7. Phase diagram that delineates where hyperbolic points exist in the fluid profile about a swimming *C. elegans*. Region I identifies points where hyperbolic points are not observed, and region II identifies points where hyperbolic points are observed. The dashed dark and solid gray outlines denote the boundaries of region II as a function of Γ and η_p for values of $\sigma_0 = 0$ and 500 Pa, respectively.

was done in Ref. 7. In the vicinity of the hyperbolic points, the magnitude of the trace of the elastic stress increases. This increase does not happen at the center of the hyperbolic points, but rather on the sides. Therefore, the elastic stress at the hyperbolic points has a sharp minimum that is flanked by regions of large elastic stress (Figure 6(b)). These hyperbolic points then represent regions where the polymer is being stretched on one side of the hyperbolic point and compressed on the other. Similar stretching and compression has been shown to occur for single elastic fibers at hyperbolic points in fluid flow.[31]

Because our two-phase IB method is able to accurately reproduce the swimming behavior of *C. elegans* through viscoelastic media, it provides a method for exploring the physics that leads to differences between swimming through viscous fluids and viscoelastic media. Here, we chose to further investigate the advent of the hyperbolic points near swimmers. Specifically, we asked what parameters are most relevant for producing hyperbolic flow profiles. In order to address this question, we varied three of the parameters that define the viscoelasticity of the medium: the polymer-fluid drag coefficient Γ, the polymer viscosity η_p, and the hydrostatic compressibility of the polymer σ_0. We then analyzed the flow patterns by eye and determined under which parameter values we found hyperbolic points that were at least half a body length away from the swimmer. In Figure 7, we show phase diagrams where the hyperbolic points are observed. When the fluid-polymer drag is moderate ($\Gamma = 1.78 \times 10^3$ Pa s/m^2), *C. elegans* generates hyperbolic points in a broad range of values of the hydrostatic compressibility and polymer viscosity. When Γ is small (1.78×10^2 Pa s/m^2), the hydrostatic compressibility has a more significant effect on the generation of hyperbolic points. When the fluid-polymer drag coefficient is large ($\Gamma = 1.78 \times 10^6$ Pa s/m^2), increases in the polymer viscosity reduce the likelihood of generating hyperbolic points. Therefore, our model suggests that an appropriate drag between the fluid and polymer phases is needed to generate hyperbolic points. Likewise, increases in the hydrostatic compressibility can also lead to hyperbolic flow profiles. These results suggest possible engineering strategies for controlling swimming speed by modifying the environment.

This article is copyrighted as indicated in the article. Reuse of AIP content is subject to the terms at: http://scitation.aip.org/termsconditions. Downloaded to IP: 128.196.189.33 On: Wed, 06 Jan 2016 19:05:57

VII. CONCLUSION

Here, we developed an immersed boundary method for fluid/structure interactions in two-phase media and showed that this method provides accurate solutions for swimming through diverse non-Newtonian environments, including viscoelastic fluids and gels. Our algorithm provides a direct way to incorporate different assumptions about the interaction between the swimmer and the polymer component of the environment, which are likely important. Since this algorithm allows one to simulate the interaction between a swimmer and a diverse range of non-Newtonian environments, it provides a robust method for investigating the physical mechanisms that lead to the complex and often contradictory dependencies of swimming speed on rheological parameters of the environment. To highlight this capability, we simulated the swimming of *C. elegans* through viscoelastic media and showed that our algorithm reproduced the experimentally measured swimming speeds and flow profiles. Of particular note, we showed that our algorithm reproduces the hyperbolic flow points that are observed when *C. elegans* swims through viscoelastic fluids. We then showed which physical parameters are responsible for the advent of these points. While the consequences of these hyperbolic points on the fluid flow are not entirely clear, we showed that they correspond with elastic compression/extension in the polymer phase of the fluid. These elastic stresses can interact with the kinematics of the swimmer to either enhance or inhibit swimming, as has been described before.[7,30]

A major benefit of our algorithm is that it allows one to model a wide range of non-Newtonian fluids. For example, during the swimming of the Lyme disease spirochete, *B. burgdorferi*, through gels and methylcellulose solutions, it was observed that the bacterium "swims without slipping" where the bacterial swimming speed is equal to the undulation wave speed. To our knowledge, no model for swimming in viscoelastic fluids or gels has yet predicted this type of behavior and the physics that leads to it remains unknown. We, therefore, expect that this methodology will provide a large step forward in developing a complete, mechanistic understanding of microorganism swimming. In addition, because the algorithm is based on a general immersed boundary framework, it can also be applied to other non-Newtonian fluid/structure interaction problems. For example, the cytoskeleton of eukaryotic cells is composed of a meshwork of actin immersed in a fluid. A number of authors have treated this system as a two-phase fluid.[14] Therefore, this algorithm may also be useful for studying eukaryotic cell crawling or any other system where solid structures are immersed in a fluid suspension.

While we focused here on 2D simulations, the algorithm is also easily extendable to 3D due to the fact that the two-phase fluid solver that we describe and the immersed boundary delta functions/smearing operators are based on standard stencils. We do not expect the results described here to be strongly altered in 3D, as it has been shown that the swimming speed of a 2D sheet problem and a 3D filament in an Oldroyd B fluid are affected in the same way by the Deborah number.[6,32]

ACKNOWLEDGMENTS

This work was supported by the National Institutes of Health Grant No. NIH R01 GM072004. P. Lee was also supported by No. NIH P50GM094503. The authors thank P. Arratia for useful discussions and the kinematic and rheological data for the swimming of *C. elegans* through viscoelastic fluids.

[1] E. A. Gaffney, H. Gadelha, D. J. Smith, J. R. Blake, and J. C. Kirkman-Brown, "Mammalian sperm motility: Observation and theory," Annu. Rev. Fluid Mech. **43**, 501–528 (2011).
[2] R. B. Kimsey and A. Spielman, "Motility of Lyme disease spirochetes in fluids as viscous as the extracellular matrix," J. Infect. Dis. **162**, 1205–1208 (1990).
[3] M. W. Harman, S. M. Dunham-Ems, M. J. Caimano, A. A. Belperron, L. K. Bockenstedt, H. Fu, J. D. Radolf, and C. W. Wolgemuth, "The heterogeneous motility of the Lyme disease spirochete in gelatin mimics dissemination through tissue," Proc. Natl. Acad. Sci. U. S. A. **109**, 3059–3064 (2012).
[4] C. Fang-Yen, M. Wyart, J. Xie, R. Kawai, T. Kodger, S. Chen, Q. Wen, and A. D. T. Samuel, "Biomechanical analysis of gait and adaptation in the nematode *caenorhabditis elegans*," Proc. Natl. Acad. Sci. U. S. A. **107**, 20323–20328 (2010).
[5] G. Taylor, "Analysis of the swimming of microscopic organisms," Proc. R. Soc. A **209**, 447–461 (1951).
[6] E. Lauga, "Propulsion in a viscoelastic fluid," Phys. Fluids **19**, 083104 (2007).
[7] J. Teran, L. Fauci, and M. Shelley, "Viscoelastic fluid response can increase the speed and efficiency of a free swimmer," Phys. Rev. Lett. **104**, 038101 (2010).

This article is copyrighted as indicated in the article. Reuse of AIP content is subject to the terms at: http://scitation.aip.org/termsconditions. Downloaded to IP: 128.196.189.33 On: Wed, 06 Jan 2016 19:05:57

[8] X. Shen and P. E. Arratia, "Undulatory swimming in viscoelastic fluids," Phys. Rev. Lett. **106**, 208101 (2011).
[9] B. Liu, T. R. Powers, and K. S. Breuer, "Force-free swimming of a model helical flagellum in viscoelastic fluids," Proc. Natl. Acad. Sci. U. S. A. **108**, 19516–19520 (2011).
[10] F. A. Godinez, L. Koens, T. D. Montenegro-Johnson, R. Zenit, and E. Lauga, "Complex fluids affect low-Reynolds number locomotion in a kinematic-dependent manner," Exp. Fluids **56**, 97 (2015).
[11] M. Doi and A. Onuki, "Dynamic coupling between stress and composition in polymer solutions and blends," J. Phys. II **2**, 1631–1656 (1992).
[12] H. Tanaka, "Viscoelastic phase separation," J. Phys.: Condens. Matter **12**, R207–R264 (2000).
[13] W. Alt and M. Dembo, "Cytoplasm dynamics and cell motion: Two-phase flow models," Math. Biosci. **156**, 207–228 (1999).
[14] N. G. Cogan and R. D. Guy, "Multiphase flow models of biogels from crawling cells to bacterial biofilms," HFSP J. **4**, 11–25 (2010).
[15] J. Du, J. P. Keener, R. D. Guy, and A. L. Fogelson, "Low Reynolds number swimming in viscous two-phase fluids," Phys. Rev. E **85**, 036304 (2012).
[16] D. A. Drew and L. A. Segel, "Analysis of fluidized beds and foams using averaged equations," Stud. Appl. Math. **50**, 233–257 (1971).
[17] C. W. Wolgemuth, "Collective swimming and the dynamics of bacterial turbulence," Biophys. J. **95**, 1564–1574 (2010).
[18] C. W. Wolgemuth, "Biomechanics of cell motility," in *Comprehensive Biophysics*, edited by E. H. Egelman, Cell Biophysics, Denis Wirtz Vol. 7 (Oxford, Academic Press, 2012), pp. 168–193.
[19] J. Happel and H. Brenner, *Low Reynolds Number Hydrodynamics* (Martinus Nijhoff Publishers, The Hague, 1983).
[20] M. A. Meyers and K. K. Chawla, *Mechanical Behavior of Materials* (Cambridge University Press, 2009).
[21] A.-K. Tornberg and M. J. Shelley, "Simulating the dynamics and interactions of flexible fibers in stokes flows," J. Comput. Phys. **196**, 8–40 (2004).
[22] H. C. Fu, V. B. Shenoy, and T. R. Powers, "Low Reynolds number swimming in gels," EPL **91**, 24002 (2010).
[23] S. Lim and C. S. Peskin, "Simulations of the whirling instability by the immersed boundary method," SIAM J. Sci. Comput. **25**, 2066–2083 (2004).
[24] D. L. Brown, R. Cortez, and M. L. Minion, "Accurate projection methods for the incompressible Navier-Stokes equations," J. Comput. Phys. **168**, 464–499 (2001).
[25] P. Lee, B. E. Griffith, and C. S. Peskin, "The immersed boundary method for advection-electrodiffusion with implicit timestepping and local mesh refinement," J. Comput. Phys. **229**, 5208–5227 (2010).
[26] S. Balay, S. Abhyankar, M. F. Adams, J. Brown, P. Brune, K. Buschelman, L. Dalcin, V. Eijkhout, W. D. Gropp, D. Kaushik, M. G. Knepley, L. C. McInnes, K. Rupp, B. F. Smith, S. Zampini, and H. Zhang, PETSc Web page, http://www.mcs.anl.gov/petsc (2015).
[27] C. S. Peskin, "The immersed boundary method," Acta Numer. **11**, 479–517 (2002).
[28] L. J. Fauci and C. S. Peskin, "A computational model of aquatic animal locomotion," J. Comput. Phys. **77**, 85–108 (1988).
[29] C. W. Wolgemuth, A. Mogilner, and G. Oster, "The hydration dynamics of polyelectrolyte gels with applications to cell motility and drug delivery," Eur. Biophys. J. **33**, 146–158 (2004).
[30] B. Thomases and R. D. Guy, "Mechanisms of elastic enhancement and hindrance for finite-length undulatory swimmers in viscoelastic fluids," Phys. Rev. Lett. **113**, 098102 (2014).
[31] Y.-N. Young and M. J. Shelley, "Stretch-coil transition and transport of fibers in cellular flows," Phys. Rev. Lett. **99**, 058303 (2007).
[32] H. C. Fu, T. R. Powers, and C. W. Wolgemuth, "Theory of swimming filaments in viscoelastic media," Phys. Rev. Lett. **99**, 258101 (2007).

This article is copyrighted as indicated in the article. Reuse of AIP content is subject to the terms at: http://scitation.aip.org/termsconditions. Downloaded to IP: 128.196.189.33 On: Wed, 06 Jan 2016 19:05:57